Efficient Computation of Dendritic Microstructures using Adaptive Mesh Refinement

Nikolas Provatas[1,2], Nigel Goldenfeld[1], and Jonathan Dantzig[2]
[1] *University of Illinois at Urbana-Champaign, Department of Physics*
1110 West Green Street, Urbana, IL, 61801
[2] *University of Illinois at Urbana-Champaign, Department of Mechanical and Industrial Engineering*
1206 West Green Street, Urbana, IL, 61801
(February 1, 2008)

We study dendritic microstructure evolution using an adaptive grid, finite element method applied to a phase-field model. The computational complexity of our algorithm, per unit time, scales linearly with system size, rather than the quadratic variation given by standard uniform mesh schemes. Time-dependent calculations in two dimensions are in good agreement with the predictions of solvability theory, and can be extended to three dimensions and small undercoolings.

05.70.Ln, 81.30.Fb, 64.70.Dv, 81.10.Aj

Dendrites are the primary component of solidification microstructures in metals. The formation, shape, speed and size of dendritic microstructures has been a topic of intense study in the past 10-15 years. Experiments [1,2] by Glicksman and coworkers on succinonitrile (SCN) and other transparent analogues of metals have been accurate enough to provide tests of theories of dendritic growth, and have stimulated considerable theoretical progress [3–5]. The experiments have clearly demonstrated that naturally growing dendrites possess a unique steady state tip, characterized by its velocity, radius of curvature and shape, which leads the to time-dependent sidebranched dendrite as it propagates.

The earliest theories of dendritic growth solved for the diffusion field around a self-similar body of revolution propagating at constant speed [6,7]. In these studies the diffusion field determines the product of the dendrite velocity and tip radius, but neither quantity by itself. Adding capillarity effects to the theory predicts a unique maximum growth speed, [8] but experiments showed that this point does not represent the operating state for real dendrites.

The goal of contemporary research has been to predict steady state features of dendritic growth and to compute time-dependent microstructures from numerical solutions of the equations of motion. The purpose of this letter is to present a computationally efficient method for time-dependent calculations, and to verify that the steady state properties are in excellent agreement with those predicted by analysis of the steady state problem.

Insight into the steady state dendrite problem was first obtained from local models [3,4,9–18] describing the evolution of the interface, and incorporating the features of the bulk phases into the governing equation of motion for the interface. These models were the first [10] to show that a nonzero dendrite velocity is obtained only if a source of anisotropy – for example, anisotropic interface energy – is present in the description of dendritic evolution. Subsequently, it was shown that the spectrum of allowed steady state velocities is discrete, rather than continuous, and the role of anisotropy was understood theoretically, both in the local models and the full moving boundary problem [4,5,14,19]. Moreover, only the fastest of a spectrum of steady state velocities is stable, thus forming the operating state of the dendrite. It is widely believed that sidebranching is generated by thermal or other statistical fluctuations on a microscopic scale, which are amplified by advective diffusion. This body of theoretical work is generally known as solvability theory.

Numerically solving the time-dependent Stefan problem, or variations of it, is difficult, requiring front tracking and lattice deformation to contain the interface at predefined locations on the grid [20]. These difficulties have been partially addressed by the introduction of the *phase-field* model, which introduces an auxiliary continuous order parameter $\phi(\mathbf{r})$ that couples to the evolution of the thermal field. The phase field interpolates between the solid and liquid phases, attaining two different constant values in either phase, with a rapid transition region in the vicinity of the solidification front. The level set of $\phi(\mathbf{r}) = 0$ is identified with the solidification front, and the dynamics of ϕ are carefully designed so that the level set dynamics follows that of the evolving solidification front [21–32]..

The phase-field model finesses the problem of front tracking, but it is still prohibitively expensive for large systems. The cost is driven by the combined requirements of fine resolution near the interface and a domain size set by the diffusion length and time for the system to evolve to steady state. The grid spacing must be small enough that the phase-field model converges to the Stefan problem, often referred to as the sharp interface limit. Recent work by Karma and Rappel [33], involving an improved representation for the temperature field within the interface, has extended this limit to the order of the capillary length, typically 10^{-8}m. While improved asymptotics does help, the large system size needed to contain large diffusion-limited structures which form at low undercoolings, and the extended time scales have remained out of reach. Unfortunately, it is precisely these conditions that prevail in the most successful experiments done to date [2].

Our contribution in this article is to show how Karma

and Rappel's phase field model can be implemented in a computationally efficient manner, thus removing a significant obstacle to the numerical solution of large-scale solidification problems. We exploit the fact that the phase and temperature fields are both essentially constant over most of space, with significant variation only near the solidification front itself. This suggests that an adaptive mesh method which concentrates grid points in the interface region will be efficient. However, the implementation is non-trivial, and we have found it effective to use finite element methods, as described below.

We first illustrate that our method allows faster and more efficient numerical integration of phase-field models, especially in large systems and integration for long times. We then examine the physics of dendritic growth using a phase-field model solved by this method. In particular, we present the convergence properties and velocity selection of dendrites. We also measure the effective anisotropy introduced by our adapting grids, and compare it to that obtained using uniform grid methods.

We model solidification using the phase-field model used by Karma and Rappel [33]. We rescale temperature T by $U = c_P(T - T_M)/L$, where c_P is the specific heat at constant pressure, L is the latent heat of fusion and T_M is the melting temperature. The order parameter is defined by ϕ, with $\phi = 1$ in the solid, $\phi = -1$ in the liquid. The interface is defined by $\phi = 0$. We rescale time by τ_o, a time characterizing atomic movement in the interface, and length by W_o, a length characterizing the narrow region between liquid and solid. The model is given by

$$\frac{\partial U}{dt} = D\nabla^2 U + \frac{1}{2}\frac{\partial \phi}{\partial t} \tag{1}$$

$$A^2(\vec{n})\frac{\partial \phi}{dt} = \nabla \cdot (A^2(\vec{n})\nabla\phi) + (\phi - \lambda U(1-\phi^2))(1-\phi^2)$$
$$+ \frac{\partial}{\partial x}\left(|\nabla\phi|^2 A(\vec{n})\frac{\partial A(\vec{n})}{\partial \phi_{,x}}\right) + \frac{\partial}{\partial y}\left(|\nabla\phi|^2 A(\vec{n})\frac{\partial A(\vec{n})}{\partial \phi_{,y}}\right),$$

where $D = \alpha\tau_o/W_o^2$ and α is the thermal diffusivity, and where λ is a parameter that controls the coupling of U and ϕ. Anisotropy has been introduced in Eqs. (1) by defining the width of the interface to be $W(\vec{n}) = W_o A(\vec{n})$ and the characteristic time by $\tau(\vec{n}) = \tau_o A^2(\vec{n})$ [33], with $A(\vec{n}) \in [0,1]$, and

$$A(\vec{n}) = (1-3\epsilon)\left[1 + \frac{4\epsilon}{1-3\epsilon}\frac{(\phi_{,x})^4 + (\phi_{,y})^4}{|\nabla\phi|^4}\right]. \tag{2}$$

The vector $\vec{n}$ in Eq. (2) is the normal to the contours of ϕ, and $\phi_{,x}$ and $\phi_{,y}$ represent partial derivatives with respect to x and y. The constant ϵ parameterizes the deviation of $W(\vec{n})$ from W_o.

Karma and Rappel [33] derived asymptotic relationships between the parameters of Eqs. (1) which allow them to operate in the sharp interface limit, where U at the interface satisfies $U_{\rm int} = -d(\vec{n})\kappa - \beta(\vec{n})V_n$, where $d(\vec{n})$ is the capillary length, κ is the local curvature, $\beta(\vec{n})$ is the interface attachment kinetic coefficient and V_n the normal speed of the interface, all assumed in dimensionless form here. In terms of Eq. (2), $d(\vec{n}) = d_o\left[A(\vec{n}) + \partial_\theta^2 A(\vec{n})\right]$, where $d_o = E_1/\lambda$, where $E_1 = 0.8839$ [33] and θ is the angle between $\vec{n}$ and the x-axis. Karma and Rappel [33] also showed that W_o, τ_o and λ can be chosen so as to simulate arbitrary values of β. In particular, choosing $\lambda = C_1 D = C_1\alpha\tau_o/W_o^2$, with $C_1 = 1.5957$, makes $\beta = 0$, a limit which is appropriate for SCN [33].

We compute four-fold symmetric dendrites in a quarter-infinite space, initiated by a small quarter disk of radius R_o centered at the origin. The order parameter is initially set to its equilibrium value $\phi_o(\vec{x}) = -\tanh((|\vec{x}| - R_o)/\sqrt{2})$ along the interface. The temperature is initialized to be everywhere equal to its far-field undercooling $U(|\vec{x}|) = c_p(T_\infty - T_m)/L = -\Delta$.

We simulate Eqs. (1) on an adaptive grid of linear isoparametric quadrilateral and triangular finite elements, formulated using Galerkin's method. Element data are arranged on a two dimensional element-quadtree data structure [34], making our code scalable. The grid is locally refined to have a higher density of elements in the vicinity of the interface of the ϕ-field, as well as in an extended region in the liquid which contains the U-field. The criterion for refinement is based on changes in fluxes of both the ϕ and U fields. Typically, the grid is adapted every 100 time steps which permits the ϕ and U fields to remain within the refined range between regridding updates. We allow a difference of at most one level of refinement between neighboring quadrilateral elements. In such a case the quadrilateral element of lower level of refinement has an extra side node. The extra nodes are resolved with triangular elements. Details of our algorithm will be presented in an upcoming publication.

When using an adaptive grid procedure, the concept of a grid spacing is replaced by that of a minimum grid spacing $\Delta x_{\rm min}$, representing the finest level of spatial resolution. We found that best convergence is obtained when the algorithm *layers* the grid so the highest density of elements appears around the ϕ interface, whose width is of order 1. The U-field ahead of the ϕ field is of order D/V_n and has smaller gradients than ϕ, and so it is encompassed by a uniform mesh of grid spacing $2\Delta x_{\rm min}$ and $4\Delta x_{\rm min}$. We found that the convergence of our solutions is relatively insensitive to $\Delta x_{\rm min}$. For a test case of dendrites grown at $\Delta = 0.55$, $D = 2$, $\epsilon = 0.05$, and integration time step $dt = 0.016$, our solutions for the steady state velocity converge to that given by solvability theory to within a few percent for $0.3 \le \Delta x_{\rm min} \le 1.6$.

Fig. 1 shows a typical dendrite 10^5 times steps into its evolution computed using our adaptive grid method. For this case, $\Delta = 0.7$, $D = 2$, $\epsilon = 0.05$, and the time step $dt = 0.016$. The system size is 800×800 with $\Delta x_{\rm min} = 0.8$. Side branching is evident, and arises due to numerical noise. About half the computational do-

main is shown. This calculation took approximately 10 cpu-hours on a Sun UltraSPARC 1200E workstation.

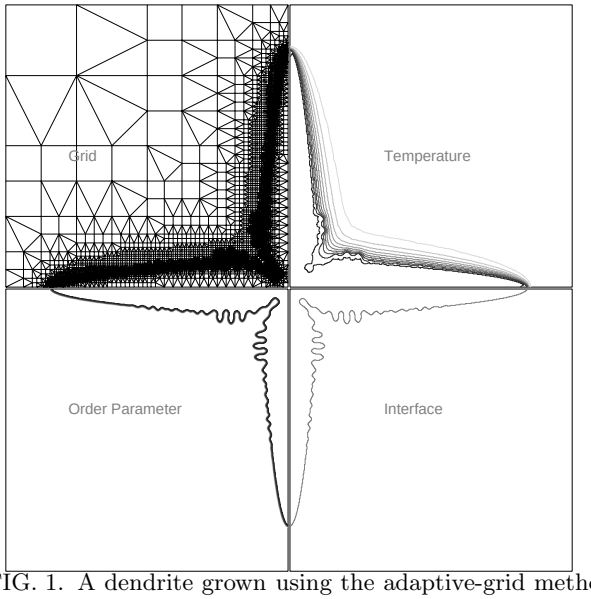

FIG. 1. A dendrite grown using the adaptive-grid method for $\Delta = 0.55$, $D = 2$, $\epsilon = 0.05$, and $dt = 0.016$. Clockwise, beginning at the upper right the figures show contours of the U-field, the contour $\phi = 0$, contours of the ϕ-field and the current mesh.

We examined the cpu-scalability of our adaptive grid algorithm with system size by growing dendrites in systems of linear dimension L_B and measuring the cpu time R_t^a for the dendrite to traverse the entire system. For $\Delta = 0.55$, $\Delta x_{\min} = 0.4$ and the other parameters the same as those used in computing Fig. 1, the relationship between R_t^a and L_B is shown in Fig. 2 where we see that $R_t^a \sim L_B^2$. The number of calculations performed, per unit time, is proportional to the number of elements in our grid, which is set by the arclength of the dendritic interface being simulated

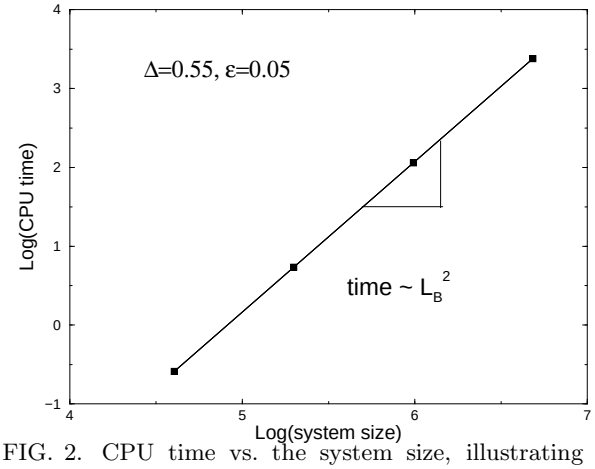

FIG. 2. CPU time vs. the system size, illustrating the quadratic dependence of computing time for a dendrite to move through the system on linear dimension L_B.

multiplied by the diffusion length D/V_n. For a parabolic shape the arclength is approximately L_B. Thus, since the dendrite moves at a constant velocity V_n,

$$R_t^a = \left[\frac{R_o^a D}{V_n^2 \Delta x_m^2}\right] L_B^2, \tag{3}$$

where R_o^a is a constant that depends on the implementation. The cpu time R_t^u needed to compute a full dendritic microstructure on a uniform grid scales as $R_t^u = [R_o^u/(V_n \Delta x_m^2)] L_B^3$. For large system sizes, our method will be faster than uniform grid methods by a factor L_B.

We tested the velocity selection mechanism of the phase-field model solved by our adaptive-grid algorithm for various undercoolings. In all cases we found very good agreement with the results of solvability theory. Fig. 3 shows the rescaled tip velocity $V_n d_o/D$ vs. time for three different undercoolings, $\Delta = 0.45, 0.55, 0.65$, with corresponding dimensionless thermal diffusivities $D = 3, 2, 1$, and dimensionless capillary length $d_o = 0.185, 0.277, 0.554$ respectively. In all cases the steady state tip velocity of our dendrite reproduces solvability theory – shown by the horizontal lines – within a few percent.

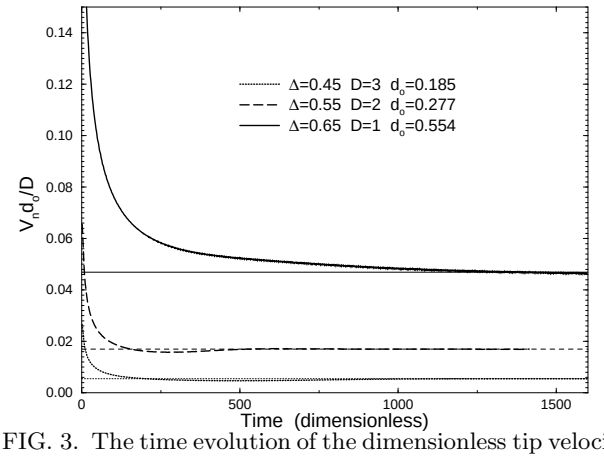

FIG. 3. The time evolution of the dimensionless tip velocity for undercooling $\Delta = 0.45, 0.55, 0.65$. The horizontal lines are the results of solvability theory.

We also tested the effective anisotropy of our dynamically adapting lattice following the method of Karma and Rappel [33]. We couple ϕ to an initially constant background temperature $\Delta_b = d_o/R_o$. This maintains the interface in equilibrium for the case of isotropic surface energy. When growing in the presence of anisotropy, Δ_b is adjusted dynamically so as to maintain the velocity of the interface, measured along the x-axis, to zero. Eventually our crystal neither shrinks nor grows, and its final equilibrium shape is fitted to the form

$$R(\theta) = R_o(1 + \epsilon_{\text{eff}} \cos\theta) \tag{4}$$

where R is the equilibrium radial co-ordinate the crystal and θ is the polar angle measured from its center. The effective anisotropy represents the modification to ϵ due to

the grid. Fig. 4 illustrates a crystal grown to equilibrium using an input anisotropy $\epsilon = 0.04$. Using to Eq. (4), we find $\epsilon_{\text{eff}} = 0.041$. This accuracy is typical.

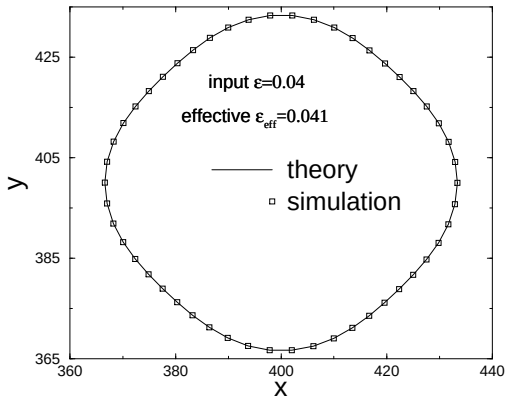

FIG. 4. The equilibrium shape of the interface, for an input anisotropy $\epsilon = 0.04$. The effective anisotropy $\epsilon = 0.041$.

This letter presents a new adaptive grid algorithm that is used to study solidification microstructures using adaptive refinement of a finite element grid. Our method is used to solve the phase-field model given by Eqs. (1). Our main result is that our solution time scales linearly with system size, rather than quadratically as one would expect in a uniform mesh. This allows us to solve the phase-field model in much larger systems and for longer simulation times. We showed that the convergence of our solutions remains accurate over a large range of Δx_m. Furthermore, dendritic tip speeds were found to be reproduced within a few percent of the theoretical values predicted by solvability theory. The effective anisotropy induced by our method was found to be a few percent of the input anisotropy. The speed increase of our method allows us to investigate dendritic microstructures at undercoolings somewhat lower than $\Delta = 0.1$ in 2D. These results, as well as work in 3D will appear in an upcoming publication.

Acknowledgements: This work has been supported by NASA Microgravity Research Program, under Grant NAG8-1249. We also thank Wouter-Jan Rappel for providing the Green's function steady-state code used to test our simulations.

[1] S.-C. Huang and M.E. Glicksman, Acta. Metall., **29**, 701 (1981)]
[2] M. E. Glicksman, Materials Science and Engineering, **65** (1984).
[3] J.S. Langer, Rev. Mod. Phys. **52**, 1 (1980);
[4] J.S. Langer, "Lectures in the Theory of Pattern Formation", in *Chance and Matter*, Les Houches Session XLVI, edited by J. Souletie, J. Vannenimus and R. Stora (North Holland, Amsterdam, 1987), p. 629.
[5] D.A. Kessler, J. Koplik and H. Levine, Adv. Phys. **37**, 255 (1988).
[6] G. P. Ivantsov, Dokl. Akad. Nauk USSR, **58**, 1113 (1947).
[7] G. Horvay and J. W. Cahn, Acta Metall. **9**, 695 (1961).
[8] D. E. Temkin, Dokl. Akad. Nauk SSSR **132**, 1307 (1960).
[9] R. Brower, D. Kessler, J. Koplik, and H. Levine, Phys. Rev. Lett., **51**, 1111, (1983).
[10] E. Ben-Jacob, N. Goldenfeld, J.S. Langer and G. Schön, Phys. Rev. Lett., **51**, 1930 (1983).
[11] E. Ben-Jacob, N. Goldenfeld, B.G. Kotliar, and J.S. Langer, Phys. Rev. Lett., **53**, 2110 (1984).
[12] A. Barbieri, D. C. Hong, and J.S. Langer, Phys. Rev. A, **35**, 1802 (1987).
[13] J.S. Langer, Phys. Rev. A, **33**, 435 (1985).
[14] E. Brener, and V. I. Melnikov, Adv. Phys. **40**, 53 (1991).
[15] D. Kessler, J. Koplik, and H. Levine, Phys. Rev. A, **30**, 3161 (1984).
[16] D. Kessler, J. Koplik, and H. Levine, Phys. Rev. A, **31**, 1712 (1985).
[17] M. Ben Amar, and E. Brener, Phys. Rev. Lett. **71**, 589 (1993).
[18] E. Brener, Phys. Rev. Lett. **71**, 3653 (1993).
[19] Y. Pomeau and M. Ben Amar, *Dendritic growth and related topics*, in *Solids far from equilibrium*, ed. C. Godrèche, (Cambridge, 1991) 365.
[20] R. Almgren, J. Comp. Phys. **106**, 337 (1993).
[21] J. S. Langer, in *Directions in Condensed Matter* (World Scientific, Singapore, 1986), 164.
[22] G. J. Fix, in *Free Boundary Problems: Theory and Applications*, Vol. II, edited by A. Fasano and M. Primicerio (Piman, Boston, 1983), 580.
[23] J. B. Collins and H. Levine, Phys. Rev. B, **31**, 6119 (1985).
[24] P. C. Hohenberg, and B. I. Halperin, Rev. Mod. Phys. **49**, 435 (1977).
[25] J. A. Warren and W. J. Boettinger, Acta Metall. Mater. A **43**, 689 (1995)
[26] A. A. Wheeler, W.J. Boettinger, and G. B. McFadden Phys. Rev. A **45**, 7424 (1992) (1996).
[27] A. Karma, Phys. Rev. E **49**, 2245 (1994).
[28] K. R. Elder, F. Drolet, J. M. Kosterlitz, and M. Grant, Phys. Rev. Lett. **72**, 677 (1994).
[29] A. A. Wheeler, G. B. McFadden, and W.J. Boettinger, Proc. Royal Soc. London A **452**,
[30] R. Kobayashi, Physica D **63**, 410 (1993).
[31] N. Provatas, E. Elder, M. Grant, Phys. Rev. B, **53**, 6263 (1996).
[32] S-L. Wang and R. F. Sekerka, Phys. Rev. E **53**, 3760 (1996).
[33] A. Karma, and W.-J. Rappel, Phys. Rev. E **53**, 3017 (1995); A. Karma, and Wouter-Jan Rappel, Preprint (1997).
[34] M. S. Shepard and J. Z. Zhu, Int. J. Numer. Math. Eng. **32**, 783 (1991).